Environmental Science & Technology

Article

Cite This: Environ. Sci. Technol. XXXX, XXX, XXX−XXX

pubs.acs.org/est

Effect of MnO_2 Phase Structure on the Oxidative Reactivity toward Bisphenol A Degradation

Jianzhi Huang,[†,§] Shifa Zhong,[†,§] Yifan Dai,[‡] Chung-Chiun Liu,[‡] and Huichun Zhang*[,†]

[†]Department of Civil Engineering and [‡]Department of Chemical & Biomolecular Engineering, Case Western Reserve University, Cleveland, Ohio 44106, United States

Supporting Information

ABSTRACT: Manganese dioxides (MnO_2) are among important environmental oxidants in contaminant removal; however, most existing work has only focused on naturally abundant MnO_2. We herein report the effects of different phase structures of synthetic MnO_2 on their oxidative activity with regard to contaminant degradation. Bisphenol A (BPA), a frequently detected contaminant in the environment, was used as a probe compound. A total of eight MnO_2 with five different phase structures (α-, β-, γ-, δ-, and λ-MnO_2) were successfully synthesized with different methods. The oxidative reactivity of MnO_2, as quantified by pseudo-first-order rate constants of BPA oxidation, followed the order of δ-MnO_2-1 > δ-MnO_2-2 > α-MnO_2-1 > α-MnO_2-2 ≈ γ-MnO_2 > λ-MnO_2 > β-MnO_2-2 > β-MnO_2-1. Extensive characterization was then conducted for MnO_2 crystal structure, morphology, surface area, reduction potential, conductivity, and surface Mn oxidation states and oxygen species. The results showed that the MnO_2 oxidative reactivity correlated highly positively with surface Mn(III) content and negatively with surface Mn average oxidation state but correlated poorly with all other properties. This indicates that surface Mn(III) played an important role in MnO_2 oxidative reactivity. For the same MnO_2 phase structure synthesized by different methods, higher surface area, reduction potential, conductivity, or surface adsorbed oxygen led to higher reactivity, suggesting that these properties play a secondary role in the reactivity. These findings provide general guidance for designing active MnO_2 for cost-effective water and wastewater treatment.

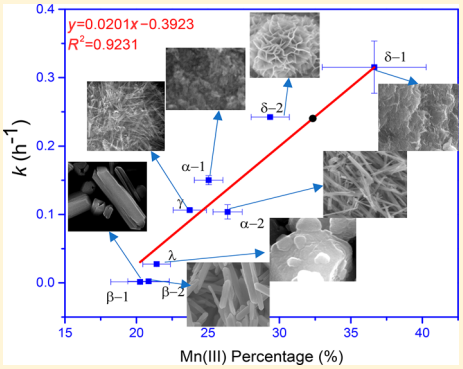

INTRODUCTION

Nowadays, the continuous release of a variety of organic contaminants (OCs) to surface and groundwater has received a great deal of attention. The persistence of these contaminants in the environment poses serious threats to ecosystems and human health. For example, the widespread of antibiotic resistance has been closely linked to the accumulation of antibiotics in the environment.[1] Endocrine-disrupting chemicals (EDCs) have deleterious effects on the normal functioning of the endocrine system in humans and wildlife.[2,3] Therefore, developing cost-effective treatment technologies to remove these contaminants is imperative. One promising technology relies on the oxidative ability of manganese dioxides (MnO_2)[4−6] because they are one of the strongest natural oxidants and are among the most-attractive oxide materials due to their high natural abundance, low cost, low toxicity, and environmental friendliness.[7−9]

MnO_2 can exist in many phase structures, such as α-, β-, γ-, δ-, and λ-MnO_2, with the same basic octahedron units [MnO_6] linked in different ways. Different phase structures of MnO_2 exhibited a wide range of catalytic activity due to different factors. For instance, α-MnO_2 was reported to have higher catalytic activity in oxygen evolution reaction (OER) than β-MnO_2, δ-MnO_2, and amorphous Mn oxide (AMO) because of its abundant di-μ-oxo bridges, low charge-transfer resistance, and strongest O_2 adsorption ability.[10] The abundance of Mn(III), the presence of mixed Mn oxidation states (III/IV), or both are often considered critical to high activity in water oxidation (WO).[10−15] However, in studies using electrocatalytic assays or chemical oxidants to examine the catalytic activity, Mn(IV) oxides exhibited higher activity than Mn_2O_3 and Mn_3O_4, implying that Mn(IV) oxides having higher activity.[16] In the total oxidation of VOCs and CO, the high catalytic activity of an octahedral molecular sieve (OMS-2) and AMO was mostly attributed to the mobility and reactivity of lattice oxygen, although other factors, including the presence of Mn(III,IV) couple, high porosity, acidity, and surface hydrophobicity, were also believed to be important.[17−20] In addition, urchin-like γ-MnO_2 was reported to be more reactive than α-, β-, and δ-MnO_2 in NO oxidation because γ-MnO_2 had more active surface oxygen species.[21]

Given the important role of structural properties in MnO_2 catalytic activity, it is highly likely that MnO_2 of different phase structures can have significantly different oxidative reactivity toward OCs. So far, naturally abundant MnO_2 have been

Received: June 20, 2018
Revised: September 4, 2018
Accepted: September 6, 2018
Published: September 6, 2018

DOI: 10.1021/acs.est.8b03383
Environ. Sci. Technol. XXXX, XXX, XXX−XXX

widely examined for removal of many OCs,[6,9,22] including phenols,[6,8,9] anilines,[23] fluoroquinolones,[24] and N-oxides.[25] These studies have evolved from investigating reductive dissolution of the oxides to quantifying contaminant transformation,[6] with focuses on changes in reaction rates with varying pH and initial reactant concentrations[5] and in the presence of cations,[4] natural organic matter (NOM),[4,6,9] or secondary metal oxides.[6,9] Many studies have also reported the products and oxidation mechanisms of the OCs.[5,22,24−26] However, most of the MnO_2 used in these studies are naturally abundant MnO_2 such as birnessite, and only a very small number of studies have compared the oxidative reactivity of different MnO_2 phase structures.[27−31] Among the latter studies, conflicting findings were reported for the effect of MnO_2 structural properties. For example, some studies showed that higher Mn average oxidation states (AOS) resulted in higher reactivity,[29,30] while others reported the opposite results.[32] Several studies discovered higher reactivity of δ- and α-MnO_2 than γ- and β-MnO_2,[37,40] while others reported that the reactivity of various MnO_2 either followed the opposite trend or was affected more by the synthesis methods than by the MnO_2 phase structure.[29,30]

Because of the complexity in and limited understanding of MnO_2 oxidative reactivity, it is imperative to systematically investigate the effect of MnO_2 phase structures on their oxidative reactivity so that MnO_2-based, cost-effective water-treatment technologies can be developed to selectively remove OCs. To this end, we examined the degradation of bisphenol A (BPA) by five different structured MnO_2, including α-, β-, γ-, δ-, and λ-MnO_2 and three Mn(III) oxides (two Mn_2O_3 and one MnOOH). BPA, one of the most frequently studied EDCs, is commonly detected in natural environments, such as wastewater, surface water, soil and sewage sludge.[33] Therefore, it was used as a chemical probe to quantify the oxidative reactivity of MnO_2. A pair of synthesis methods were followed for α-, β-, and δ-MnO_2 to examine the effect of different synthesis approaches. Various characterization techniques, including X-ray powder diffraction (XRD), scanning electron microscopy−energy-dispersive X-ray spectroscopy (SEM/EDX), high-resolution transmission electron microscopy (HRTEM), X-ray photoelectron spectroscopy (XPS), cyclic voltammetry (CV), and electrochemical impedance spectroscopy (EIS), were employed to examine the oxide morphology, structural properties, and surface composition. Correlations between the observed activity and surface and structural properties were then conducted to understand the most important factors for the reactivity. Finally, the impact of the most important factor, Mn(III) contents, and several secondary factors were discussed and compared to the reported catalytic activity of various MnO_2 values.

EXPERIMENTAL SECTION

Details on the chemical reagents and MnO_2 synthesis methods and some additional details regarding characterization techniques are listed in the Supporting Information.

BPA Oxidation Kinetics. All kinetic experiments were conducted in duplicates in 50 mL amber bottles with Teflon caps. The reaction bottles were continuously stirred on a magnetic stir plate at room temperature (23 ± 2 °C). The reaction solutions were maintained at pH 5.0 using 25 mM acetate buffer. 0.01 M NaCl was added to maintain the ionic strength. Reactions were initiated by adding a known amount of BPA to the reactors. Aliquots of samples were collected at predetermined time intervals and quenched with excess amounts of L-ascorbic acid to rapidly convert the remaining MnO_2 to Mn(II) ions. The concentration of BPA in the solution was analyzed by an Agilent 1260 Infinity II reverse-phase high-performance liquid chromatography (HPLC) system with a diode array detector, and a Zorbax XDB-C18 column (4.6 × 250 mm, 5 μm) at a flow rate of 1 mL/min. The mobile phase was methanol and 0.1% acetic acid (57:43). Rate constants for the oxidative reactivity (k) were calculated based on the pseudo-first-order kinetics.

Characterization. X-ray diffraction (XRD) data were collected using a Bruker D8 Advance powder X-ray diffractometer with Cu Kα radiation (λ = 0.154056 nm) at a beam voltage of 40 kV and a 40 mA beam current. XRD scans were collected over the 2θ range of 10°−60° with a step size of 0.05° and a sampling time of 2 s per step. The Brunauer−Emmett−Teller (BET) specific surface areas were determined by nitrogen adsorption−desorption isotherms that were measured on a Micrometritics TriStar II instrument. XPS was done on a PHI VersaProbe 5000 Scanning XPS instrument using a monochromatic Al Kα radiation as the radiation source operating at 25 W. Spectra of standard manganese oxides (MnO, Mn_2O_3, and MnO_2) were recorded under the same conditions. For each structure, triplicate samples were analyzed. Data analysis and curve fitting were performed using MultiPak XPS software following previous work by Cerrato et al.[22,34] HRTEM images were collected using a Tecnai TF30 ST transmission electron microscope, and SEM images and EDX were recorded using a FEI Quanta 400F scanning electron microscope operated under a high-vacuum mode. The electrochemical studies were conducted in a three-electrode configuration electrochemical cell using 0.5 M phosphate buffer (pH ≈ 7.0) or 0.5 M Na_2SO_4 buffered in a 10 mM HAc-NaAc buffer solution at pH 5. Bulk Mn AOS was determined by chemical titration following a previous paper.[35]

RESULTS AND DISCUSSION

Characterization of MnO_2 Materials. The phase structures of the eight synthesized MnO_2 were confirmed by the XRD patterns (Figure 1), in which the peak positions of each MnO_2 sample were precisely fitted to the corresponding

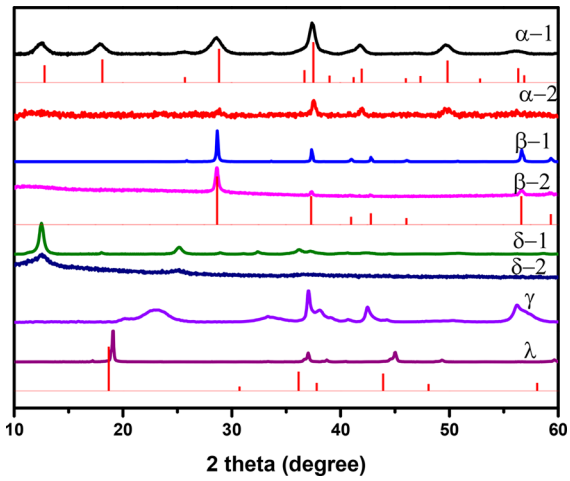

Figure 1. XRD patterns of different MnO_2 structures. The vertical lines are the corresponding standard patterns for the MnO_2 in the inorganic crystallographic database.

DOI: 10.1021/acs.est.8b03383
Environ. Sci. Technol. XXXX, XXX, XXX−XXX

Table 1. BET Surface Area, Mn Average Oxidation State, Surface Mn and O Chemical Composition, Reduction Potential (E_0), and Oxidative Reactivity of MnO_2

MnO_2	surface area (m^2/g)	AOS[a]	AOS[b]	percent Mn(III)[c]	E_0 (V)	percent O_{sur}[d]	percent O_{latt}[d]	K/Mn[e]	ratio[f]
α-MnO_2-1	175	3.67 ± 0.04	3.72 ± 0.11	25.1 ± 1.0	0.665	14.2 ± 0.9	85.8 ± 0.9	0.12	1.07
α-MnO_2-2	74	3.72 ± 0.04	3.67 ± 0.04	26.4 ± 1.0	0.642	11.0 ± 3.9	89.0 ± 3.9	0.10	1.36
β-MnO_2-1	18	3.86 ± 0.03	3.80 ± 0.07	20.3 ± 2.1	0.583	19.7 ± 3.2	80.4 ± 3.2	0	1.69
β-MnO_2-2	168	3.81 ± 0.05	3.92 ± 0.09	20.9 ± 1.5	0.585	15.1 ± 3.7	84.9 ± 3.7	0	15.23
δ-MnO_2-1	106	3.56 ± 0.05	3.49 ± 0.14	36.6 ± 3.6	0.632	15.2 ± 2.8	84.8 ± 2.8	0.27	1.52
δ-MnO_2-2	34	3.58 ± 0.03	3.64 ± 0.07	29.4 ± 1.3	0.618	12.4 ± 0.8	87.6 ± 0.8	0.24	1.38
γ-MnO_2	73	3.78 ± 0.03	3.83 ± 0.07	23.7 ± 1.2	0.585	20.9 ± 2.2	79.1 ± 2.2	0	1.94
λ-MnO_2	8	3.74 ± 0.05	3.94 ± 0.03	21.4 ± 1.0	0.559	24.0 ± 3.9	69.9 ± 2.6	0	2.07

[a]Obtained from Mn 3s multiplet splitting. [b]Obtained from chemical titration. [c]Percentage compositions of Mn 3p spectra by fitting Mn(II), Mn(III), and Mn(IV). [d]Percentage compositions of O 1s spectra by fitting O_{water}, O_{sur}, and O_{latt}. [e]The ratio of K to Mn was obtain by EDX. [f]The ratio of the pseudo first-order kinetics rate constants of MnO_2 in the presence of pyrophosphate (PP) vs that of MnO_2 alone. Conditions: [MnO_2] 138 μM; BPA 6 μM; [NaCl] 0.01 M; PP 20 μM; pH 5.

standard patterns in the inorganic crystallographic database or previous reports.[10,16] However, their peak intensities and shapes (e.g., narrow or broad) differed distinctly from each other even for the same phase structure, which were mainly attributed to their intrinsic discrepancy as well as different synthesis methods. α-, β-, and λ-MnO_2 have high crystallinity based on their narrow peak width and high intensities. δ-MnO_2 demonstrated much-broader and weaker XRD peaks than those of α- and β-MnO_2 because δ-MnO_2 generally has disordered structures in certain crystallographic directions.[36,37] Similar to δ-MnO_2, γ-MnO_2 also showed low crystallinity because it is typically the product of irregular intergrowth of elements of ramsdellite and pyrolusite.[37,38] This was further confirmed by HRTEM (Figure S1), in which vague lattice lines with partial disorder were observed for δ-MnO_2-1, δ-MnO_2-2, and γ-MnO_2, while easily recognized lattice lines with fine regular arrangement were found in α-MnO_2, β-MnO_2, and λ-MnO_2.

For the same structures (e.g., α-MnO_2-1 and α-MnO_2-2), the differences in peak shapes and intensities were mainly due to the different synthesis methods. The effect of synthesis methods is fully reflected in the morphologies of the MnO_2 (Figure S1), in which various morphologies with different sizes were obtained, including particle (α-MnO_2-1 and λ-MnO_2), needle or fiber (α-MnO_2-2 and γ-MnO_2), rod (β-MnO_2-1 and β-MnO_2-2), sheet (δ-MnO_2-1), and flower-shape (δ-MnO_2-2). These differences in morphology would directly result in differences in the BET surface areas (Table 1). Other physicochemical properties were also examined and listed in Table 1 (details in sections below). There is a slight difference in many physicochemical properties for the same structured MnO_2, such as surface adsorbed oxygen (O_{surf}), lattice oxygen (O_{latt}) species and Mn(III) contents in pairs of α-MnO_2, β-MnO_2, and δ-MnO_2; so are the properties of E_0, AOS, and K/Mn (Table 1). The relationship between these structural properties and their oxidative reactivity will be discussed in detail below.

Kinetics of BPA Oxidation by Different MnO_2. As shown in Figure 2 and Table S1, δ-MnO_2-1 has the highest reactivity, while the reactivity of both β-MnO_2 is very low. The reactivity decreases in the order: δ-MnO_2-1 > δ-MnO_2-2 > α-MnO_2-1 > α-MnO_2-2 > γ-MnO_2 > λ-MnO_2 > β-MnO_2-2 > β-MnO_2-1. Dong et al. found similar results showing the oxidative degradation of 2-mercaptobenzo-thiazole following the order: δ-MnO_2 (CM) > α-MnO_2 (CM) > α-MnO_2 (OM) > γ-MnO_2 (OM) > β-MnO_2 (OM)-2, where CM and OM

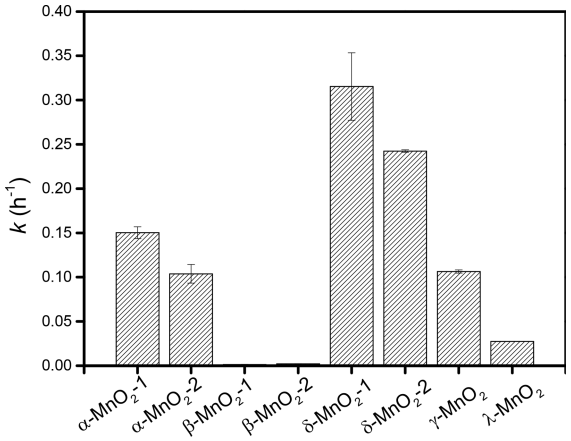

Figure 2. Pseudo-first-order oxidation rate constants (k) of BPA by different MnO_2 structures at pH 5. Error bars are the standard deviation of duplicate samples. Conditions: [MnO_2] 138 μM; BPA 6 μM; [NaCl] 0.01 M.

stand for two MnO_2 synthesis methods: comproportionation and liquid-phase oxidation, respectively.[31] However, some previous studies have shown different orders of MnO_2 oxidative reactivity when other OCs were used to examine the reactivity: (1) Liu et al. found that the oxidative reactivity of sulfadiazine by MnO_2 followed the order: δ-MnO_2−II > α-MnO_2−II > α-MnO_2−III > β-MnO_2−I > γ-MnO_2 > δ-MnO_2−I > β-MnO_2−II > α-MnO_2−I.[30] The rate constant values correlated positively with AOS and reduction potentials of the MnO_2 but negatively with pHzpc and apparent activation energy. (2) The oxidative reactivity of 2-mercaptobenzo-thiazole by MnO_2 followed the order: γ-MnOOH > β-MnO_2 > γ-MnO_2 > α-MnO_2 > δ-MnO_2, which were attributed to different specific surface areas and reduction potentials.[29] Moreover, Wan et al. showed that the α-MnO_2 synthesized at 150 °C exhibited the highest degradation rate of sulfamethoxazole (compared to other synthesis temperatures between 130 and 210 °C), due to the crystallographic structure, Mn(III) contents and labile oxygen species.[39] To have a systematic understanding of the factors governing MnO_2 oxidative reactivity, a number of physiochemical and structural parameters of the oxides were investigated, as shown below.

Effects of Surface Area and Reduction Potential. It is generally thought that the catalytic and oxidative reactivity of MnO_2 is highly dependent on its surface area. For instance, it has been reported that the degradation rate of 2-mercapto-

DOI: 10.1021/acs.est.8b03383
Environ. Sci. Technol. XXXX, XXX, XXX−XXX

benzo-thiazole by manganese (hydro)oxides was positively correlated with specific surface area.[29] Shin et al. showed that higher surface areas of manganese oxides resulted in faster degradation of atrazine due to an increase in available reactive sites.[28] The BET surface area of the eight MnO_2 varied from 8 to 175 m^2/g (Table 1). α-MnO_2-1 has the largest surface area, while λ-MnO_2 has the smallest. However, unlike these previous studies,[28,29] we observed a poor linear relationship between surface area and reactivity (Figure S2, $R^2 = 0.01$), suggesting surface area is not the major reason for the different reactivity observed. For example, the surface area of δ-MnO_2-1 (106 m^2/g) is smaller than that of β-MnO_2-2 (168 m^2/g), but its oxidative reactivity is about 150 times faster. When comparing the same structured MnO_2 prepared by two different methods, however, the ones with higher surface areas showed higher reactivity, i.e., α-MnO_2-1 > α-MnO_2-2, β-MnO_2-2 > β-MnO_2-1, and δ-MnO_2-1 > δ-MnO_2-2. Therefore, surface area seems to be a secondary parameter determining MnO_2 reactivity. Previous studies that reported that surface area is the major reason for the oxidative reactivity should be limited to the types of oxides involved.

It is commonly accepted that oxidants with higher E_0 values yield higher oxidative reactivity. For instance, the initial reaction rate of phenol by manganese oxides increased with increasing reduction potential.[27] In addition, Liu et al. showed that higher reduction potential would lead to higher oxidative reaction rates by manganese (hydro)oxides.[29] To investigate the importance of reduction potential to MnO_2 oxidative reactivity, the CV of different MnO_2-modified glassy carbon electrodes were obtained (Figure S3). The cathodic current reduction peak (E_{pc}) is related to the reduction of Mn(IV) or Mn(III) to Mn(II). α-MnO_2-1 showed a reduction peak at the highest positive potential (E_0 = +0.665 V), indicating α-MnO_2-1 had the highest oxidative capability among the eight MnO_2. The observed peak E_0 values decreased in the following order: α-MnO_2-1 > α-MnO_2-2 > δ-MnO_2-1 > δ-MnO_2-2 > γ-MnO_2 = β-MnO_2-2 > β-MnO_2-1 > λ-MnO_2 (Table 1). However, unlike these previous studies,[27,30] we observed a poor linear relationship between the oxidative reactivity and E_0 (Figure S4, $R^2 = 0.37$). For the same structured MnO_2 but synthesized by different methods, the ones with higher E_0 showed higher reactivity, i.e., α-MnO_2-1, β-MnO_2-2, and δ-MnO_2-1, which also indicates that E_0 is a secondary parameter affecting the redox reactivity of MnO_2.

Electrochemical Impedance Spectroscopy (EIS) of MnO_2. It has been reported that in aqueous oxidation by MnO_2, the first step is adsorption of the OCs by the MnO_2 surface, and the rate of electron transfer from the adsorbed compound to MnO_2 is the rate-limiting step for a number of compounds.[5] Furthermore, redox reaction involving Fe(III) minerals demonstrated that electrons may be transferred from one surface site to another (remote) site through the bulk conduction band.[40−42] As a result, the interfacial conductivity of the mineral may be important in the overall reaction because more-conductive minerals will lead to faster electron transfer. For instance, the highest OER activity of α-MnO_2 (> AMO > β-MnO_2 > δ-MnO_2) was partially attributed to its lowest charge-transfer resistance.[10] It is yet unclear whether the interfacial conductivity of MnO_2 is involved in the surface-involved oxidation of adsorbed contaminants. If that is the case, MnO_2 with higher conductivity will likely yield higher oxidative reactivity due to facilitated electron-transfer rates of different MnO_2. To evaluate the importance of interfacial conductivity in the electron transfer rates of different MnO_2, EIS, a useful tool with which to study the interfacial property of modified electrodes, was employed.

Phosphate buffer solution was used as the electrolyte in the electrochemical cell to support electron transfer between the working and counter electrode. The immobilized MnO_2 film would not react with the electrolyte, so an equivalent circuit with $C_2/R_2 + R_1$ (inset in Figure 3) was applied to model the

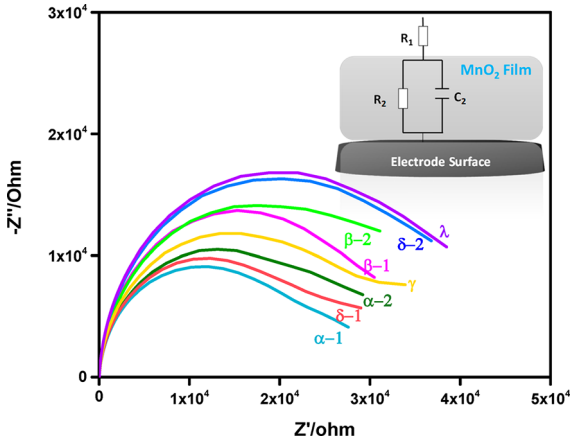

Figure 3. Nyquist plots obtained from EIS measurements of the MnO_2. Inset: equivalent circuit used to obtain charge-transfer resistance of different structured MnO_2.

conductive behavior of the MnO_2 films on the electrode surface (C_2/R_2) and the solution resistance (R_1). The electrochemical cell conditions ensured that the derived circuit model provided an accurate comparison of the conductivity of the MnO_2 without consideration of relative reaction between the MnO_2 and the phosphate buffer. The numerical values of resistance and capacitance were obtained through EC-Lab software and shown in Table S2. The impedance shown in the high-frequency region is related to the uncompensated solution resistance (R_1), which is comparable for all MnO_2. Based on the EIS spectra, the conductivity as indicated by the R_2 values decreases in the following order: α-MnO_2-1 > δ-MnO_2-1 > α-MnO_2-2 > γ-MnO_2 > β-MnO_2-1 > β-MnO_2-2 > δ-MnO_2-2 > λ-MnO_2. The measured conductivity values showed a poor linear correlation with the MnO_2 reactivity (Figure S5, $R^2 = 0.10$), suggesting that interfacial conductivity, unlike for Fe(III) minerals, is not important in the electron-transfer process between the adsorbed contaminants and MnO_2 surfaces. However, when comparing the same structured MnO_2, we found that for α- and δ-MnO_2, higher conductivity did result in higher oxidative reactivity, i.e., α-MnO_2-1 and δ-MnO_2-1. These results suggest that interfacial conductivity is another secondary parameter in MnO_2 reactivity. The conductivity of β-2 is slightly smaller than that of β-1, and the higher observed reactivity of β-2 was probably due to its much higher surface area, which masked the effect of conductivity.

Effect of Various Oxygen Species. Oxygen species play an important role in the oxidative and catalytic reactivity of MnO_2.[39,43−46] In oxidation of benzene under oxygen-free conditions, up to 3% lattice oxygen in a MnO_2 was consumed.[18] In the MnO_2-catalyzed oxidation of VOCs and CO by O_2, once the lattice oxygen is desorbed to form framework oxygen vacancies, the Mn AOS is reduced and the desorbed oxygen can directly oxidize VOCs and CO.[18] Higher

DOI: 10.1021/acs.est.8b03383
Environ. Sci. Technol. XXXX, XXX, XXX−XXX

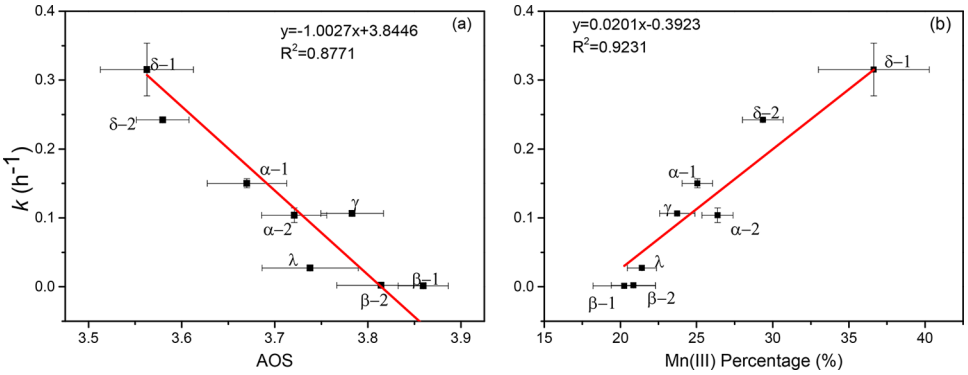

Figure 4. Relationship between pseudo-first-order rate constants k for the oxidative reaction of BPA and (a) average oxidation state based on Mn 3s fitting and (b) Mn(III) percentage.

lattice oxygen contents were reported to result in higher CO and VOCs oxidation.[37,43,47] However, in direct oxidation of OCs such as sulfamethoxazole in aqueous solution, adsorbed oxygen species (O_{sur}) instead were found to play a crucial role in the oxidation reaction, likely due to its high mobility.[39] For reactions in aqueous solution, lattice oxygen is unlikely to be replenished by O_2 under room temperature, and Mn should be the electron-transfer center because reduced Mn species typically formed after the reaction.[24]

Usually, O 1s spectra are used to identify the types of surface oxygen species present in oxide materials. All of the O 1s spectra can be clearly fitted into three peaks (Figure S6). The high binding-energy peak at 533.0 eV is assigned to the adsorbed molecular water, and the medium binding energy (531.0−532.0 eV) is assigned to O_{sur} species, while the low binding energy (529.0−529.8 eV) is attributed to O_{latt} species.[39,48] Unlike the study that observed the important contribution of O_{sur} to the oxidative reactivty,[39] we found that the order of MnO_2 reactivity did not linearly correlate with either the O_{sur} species (Figure S7, R^2 = 0.23) or the O_{latt} species (Figure S8, R^2 = 0.21) in these eight MnO_2 samples. Interestingly, when restricted to the same structured MnO_2, both α- and δ-MnO_2 that have higher O_{sur} species (i.e., α-MnO_2-1 and δ-MnO_2-1, Tables 1 and S1) were more reactive, indicating the important role of surface adsorbed oxygen in the direct oxidation reactions.[39,48] Similar to the conductivity, the much-larger surface area of β-2 masked the effect of the smaller fraction of O_{sur} species on its reactivity.

Effect of Mn AOS and the Abundance of Surface Mn(III) on the Reactivity. The AOS of Mn in MnO_2 is an important parameter that can affect its catalytic and oxidative reactivity.[49] For example, McKendry et al. found that lower Mn AOS would improve WO catalysis,[49] while Liu et al. demonstrated that higher Mn AOS of MnO_2 favored faster oxidative degradation of sulfadiazine.[30] Therefore, it would be interesting to study how Mn AOS affects the reactivity of the eight synthesized MnO_2. Here, the AOS of MnO_2 were determined by Mn 3s spectra because it is very sensitive to the AOS of Mn.[39] Calculation of AOS is shown in the following equation: AOS = 8.95−1.13ΔEs,[50] where ΔEs is the energy difference between the main peak and its satellite in Mn 3s.[39,50] Based on this equation and the values of ΔEs (Figure S9), the Mn AOS for α-1, α-2, β-1, β-2, δ-1, δ-2, γ-, and λ-MnO_2 is 3.67, 3.72, 3.86, 3.81, 3.56, 3.58, 3.78, and 3.74 eV, respectively (Table 1). The determined Mn AOS values for all MnO_2 samples are below its limit value of +4, which agrees well with previous reports.[10,39,51−53]

It has been shown that sulfadiazine oxidative degradation rates by MnO_2 strongly depended on Mn AOS, such that higher Mn AOS resulted in higher reactivity.[30] However, we found that the MnO_2 with lower AOS were more reactive. As shown in Figure 4a, there is a strong negative correlation between reactivity and AOS of MnO_2, which is similar to a previous study in which the Cr^{3+}-oxidizing ability by MnO_2 was mostly related to the presence of Mn(III).[32] The presence of Mn(III) would lead to lower AOS. Not only affecting oxidative reactivity of MnO_2, lower Mn AOS would also favor their catalytic oxidation as MnO_2 with lower AOS was more active in catalytic ozonation than that with higher AOS.[52] Ian et al. also demonstrated that birnessite with lower AOS is a key to WO catalysis.[49]

Note that different researchers have different opinions on what the best method is to measure Mn AOS.[51] Therefore, we employed two other methods to obtain Mn AOS, i.e., chemical titration for bulk AOS and Mn 3p fitting results (details below), as the results shown in Tables 1 and S1. The relationships between reactivity and Mn AOS by both approaches are shown in Figure S10, with R^2 values of 0.8011 and 0.5336 for chemical titration and Mn 3p fitting, respectively. For the chemical titration method, we still see a strong linear relationship between them, while for the Mn 3p fitting method, the linear relationship seemed to be weaker; however, it is still better than all other parameters discussed above, indicating the strong dependence of reactivity on Mn AOS. Lower Mn AOS results from the presence of Mn(II) or Mn(III) in manganese dioxides. To obtain the distribution of different Mn oxidation states (i.e., II, III, and IV) on MnO_2 surfaces and investigate the importance of surface Mn(III) to the oxidative reactivity, Mn 3p spectra were obtained, similar to a previous study.[22]

Based on the Mn 3p spectra (Figures S11 and S12), δ-MnO_2-1 has the highest percentage of Mn(III) content (36.6%, Table 1), while β-MnO_2-1 has the lowest Mn(III) content (20.3%, Tables 1 and S1). As shown in Figure 4b, there is a strong positive correlation between Mn(III) content and reactivity, which is similar to previous studies reporting that the abundance of Mn(III) is important in oxidation of environmental contaminants by δ-MnO_2.[32,54,55] Higher fractions of Mn(III) in MnO_2 will lead to lower AOS; thus, these two correlations are related. Previous work has reported the AOS of MnO_2 in WO catalysis varied from 3.3 and 3.9.[10,11,51−53,56] The role of Mn(III) will be further discussed below.

DOI: 10.1021/acs.est.8b03383
Environ. Sci. Technol. XXXX, XXX, XXX−XXX

Multiple Linear Regression Analysis. So far, we found that the Mn(III) abundance and Mn AOS are two most important factors affecting the oxidative reactivity of MnO_2. Other factors, including surface area, E_0, conductivity, and O_{surf} are secondary factors that also affect the reactivity to some extent. Therefore, multiple linear regression analysis was conducted to quantitatively examine the contribution of each parameter. The pseudo-first-order rate constant (k) is the responsive variable, while all of the factors are the predictor variables. The Mn(III) abundance and AOS are highly linearly correlated; therefore, AOS was excluded from the analysis to avoid overprediction. The model with the lowest value of Mallows's Cp is often selected as the best regression model.[57] As shown in Table S3, Model 1 with Mn(III) abundance as the sole predictive variable has the lowest Cp value (0.3), while adding any additional predictive variable would increase the Cp value. The multiple linear regression analysis thus proved that Mn(III) is the primary factor in determining the oxidative reactivity of these eight MnO_2. A pair of additional types of correlations were also conducted. First, we tried to normalize all the k values to the respective surface area to see if the surface-area-based k had any linear correlation with other parameters. Second, we tried to correlate log k with log(parameters) to see if there was any linear free-energy relationship. Both correlations are much poorer than the one above and thus are not further considered (data not shown).

Critical Role of Mn(III). The critical role of Mn(III) in catalytic activity of various MnO_2, irrespective of the crystallographic structure of the catalyst, has been well-documented.[11,15,58] This is mainly because Mn(III) has d^4 ions in the $t_{2g}^3e_g^1$ state. The anti-bonding e_g^1 electron leads to longer (Jahn−Teller distorted) and, hence, weaker Mn−O bonds than Mn(IV) (d^3). These weaker Mn−O bonds in edge sharing octahedra at the surface were believed to lead to the much higher catalytic activity of Mn_2O_3, Mn_3O_4, and λ-MnO_2 than pure α-, β-, R-, and δ-MnO_2 in WO.[15] The e_g^1 electron in the antibonding orbital can be readily donated during the reaction.[58] Indeed, when the MnO_2 surface was modified with an amine-based polymer, the formed N−Mn bonds were believed to stabilize the surface-associated Mn(III) and hence significantly lowered the onset potentials of O_2 evolution, which improved the MnO_2 catalytic activity in WO.[59] When gold nanoparticles or Cs were doped into MnO_2, the improved WO catalytic activity correlated strongly with the formation of additional surface Mn(III) species.[60,61]

Mn(III) plays not only an important role in MnO_2 when used as catalysts but also a strong and important oxidant in one electron-transfer reaction (eqs 1 and 2 versus 3),[62] and has been shown to play an important role in water treatment and biogeochemical redox processes:[63,64]

$$Mn(III) + e^- \rightarrow Mn(II) E^0 = +1.51V \quad (1)$$

See ref 65 for more information.

$$MnOOH + 3H^+ + e^- \rightarrow Mn(II) + 2H_2O E^0 = +1.50V \quad (2)$$

See ref 65 for more information.

$$MnO_2 + 4H^+ + 2e^- \rightarrow Mn(II) + 2H_2O E_0 = +1.29V \quad (3)$$

See ref 66 for more information.

Mn(III) oxides or complexes have been demonstrated to be able to rapidly oxidize a variety of OCs.[54,55,67−70] The long Mn−O bond and the antibonding electron in surface Mn(III) may facilitate fast electron transfer between the MnO_2 and the OC. Mn(III) likely accepts an electron by direct coordination with BPA through its empty σ orbital ($t_{2g}^3e_g^1 \rightarrow t_g^3e_g^2$) without change in the Mn spin state.[27] In contrast, Mn(IV) would have to undergo outer sphere electron transfer ($t_{2g}^3 \rightarrow t_{2g}^3e_g^2$) during oxidation, which requires a change in the Mn spin state, making the oxidation more difficult.[27] Therefore, it is not surprising that we observed a strong positive correlation between the surface Mn(III) content and the oxidative reactivity of the MnO_2. Based on this result, it is natural to ask whether Mn(III) oxides are more reactive than mixed Mn(III, IV) oxides. For this purpose, three Mn(III) oxides were synthesized (Text S2) and tested for their oxidative reactivity, including Mn_2O_3-1, Mn_2O_3-2, and MnOOH. Interestingly, the reactivity of these three Mn(III) oxides was much less than both δ-MnO_2 and comparable to or less than the two α-MnO_2 (Figures 3 and S13). This comparison strongly suggests the importance of Mn mixed valence (III/IV) to MnO_2 oxidative reactivity, not just the presence of Mn(III) itself, similar to what has been reported in MnO_2 catalytic activity.[10−14,71]

Due to its tetragonally distorted electron configuration, aqueous Mn(III) ions are known to be unstable against disproportionation to yield Mn(IV) solids and dissolved Mn(II) ions:[65]

$$2Mn(III) + 2H_2O \rightarrow Mn(II) + MnO_2 + 4H^+ \quad (4)$$

To test if stabilization of surface Mn(III) intermediates could improve the oxidative reactivity, pyrophosphate (PP), a well-known ligand that has a large complexation constant with Mn(III) to stabilize it, was used to examine how it affects the oxidative reactivity. As shown in eqs 1 and 2, Mn(III)/Mn(II) has a higher reductive potential than Mn(IV)/Mn(II), which would increase the reactivity when Mn(III) is stabilized. Indeed, we observed that PP enhanced the oxidative reactivity of MnO_2 by 1.06−2.07 times for all MnO_2 except for β-MnO_2-2, which is about 15 times that value (Tables 1 and S1). Previously, Gao et al. showed that PP could greatly enhance the oxidation of triclosan by MnO_2 due to the formation of strong Mn(III)−PP complexes.[72] A recent study also reported that Mn(III)−PP complexes served as a strong oxidant to induce rapid UO_2 dissolution.[69] The addition of PP into MnO_2 should mainly stabilize the intermediate Mn(III) formed during the reductive dissolution of Mn(IV)O_2, validating the important role of Mn(III) in the oxidative reactivity of MnO_2. The reason that PP enhanced the reactivity of β-MnO_2-2 by a factor of 15 is likely due to the poor reactivity of β-MnO_2-2 alone and its high surface area (168 m^2/g, Table 1) to allow significant interaction with PP.

For the types of Mn(III), Peng et al. reported that not all Mn(III) are equally reactive, and nonuniform distribution of Mn(III), i.e., more-abundant surface Mn(III) than bulk Mn(III), led to an internal potential step that allowed easy switching of the oxidation state between Mn(III) and Mn(IV).[13] Such oxidation-state switching of Mn would make it easier for an electron to transfer between Mn ions in the surface and bulk structure, thus yielding high OER catalytic activity. We believe that not only is the amount and availability of Mn(III) important, but also, different types of Mn(III) species on MnO_2 surfaces may have different reactivity. For

DOI: 10.1021/acs.est.8b03383
Environ. Sci. Technol. XXXX, XXX, XXX−XXX

example, the amounts of Mn(III) on both α-MnO_2 are comparable; however, the reactivity of α-MnO_2-1 is about 1.5 times higher than that of α-MnO_2-2 (Table 1). In addition, both β-MnO_2 have around 20% of Mn(III) (Table 1), but they were both poorly reactive. It seems like the Mn(III) in both β-MnO_2 did not contribute to the reactivity. Therefore, the redox reactivity of Mn(III) species may be different, agreeing with the literature findings.[73−75] For instance, different Mn sites, including Mn(III, IV) in MnO_2 sheets, Mn(III, IV) at the particle edges, and Mn(III) in interlayers, have been reported to have different oxidizing capacities.[73,74] Simanova et al. found that cobalt oxidation by δ-MnO_2 resulted from Mn valence and crystallographic locations: Mn(III) at the edges contributed to the redox reaction at short times, while Mn(III, IV) in the MnO_2 sheets is important at longer reaction times.[75] Manceau et al. proposed that both layer and interlayer Mn(III) in buserite would contribute to Co oxidation,[73] while other studies indicated the interlayer Mn(III) is the dominant oxidizing surface site.[74] Peng et al. even reported that the birnessite samples were almost inactive in OER activity when the abundance of Mn(III) (in total Mn) was below 12% and became very reactive as the abundance of Mn(III) increased to between 15 and 20%.[13] Therefore, we speculate that the ratio of Mn(III) to Mn(IV) might play an important role in the oxidative reactivity, and MnO_2 with a Mn AOS close to 4 may be much less reactive than those with mixed Mn(III)/Mn(IV). However, it is unclear which Mn(III)/Mn(IV) ratio is the best for the oxidative reactivity, which warrants future research. In addition, it is possible that the different reactivity of surface and structural Mn(III) resembles the different reactivity of various soluble Mn(III)−ligand complexes toward OCs.[72] It is likely the different bonding environments of Mn(III), e.g., complexation with different ligands in soluble Mn(III) complexes versus bonding to oxygen atoms in MnO_6 octahedra in geometrically different solid MnO_2, affect its stability and activity and, hence, its ability to participate in electron transfer. One caution is that the above conclusions cannot be simply extrapolated to other reaction systems containing different contaminants, especially contaminants with different reactive functional groups because different catalytic reactivity was reported for Mn oxides tested in different systems.[16] Therefore, future research should be carried out to examine if the above findings can be universally true for other reaction systems.

Role of MnO_2 Structures. Our results showed that the oxidative reactivity of layered δ-MnO_2 is better than tunnel structured MnO_2 due to more accessible active sites, which is similar to previous studies on OER.[76] In the three tunnel-structured MnO_2 investigated, β-MnO_2 has corner-shared MnO_6 and only forms small tunneled structures (1 × 1) that cannot accommodate extra water molecules and cations;[77,78] hence, it has the lowest oxidative reactivity. α-MnO_2 has larger (2 × 2) tunnels and is a combination of edge-shared and corner-shared MnO_6. γ-MnO_2 has both edge- and corner-sharing MnO_6 and has (1 × 1) tunnels of pyrolusite and (1 × 2) tunnels of ramsdellite.[79] For tunnel-structured MnO_2, the oxidative reactivity of α- and γ-MnO_2 is much higher than that of the single-tunnel structured β-MnO_2, mostly due to the more exposure of MnO_6 edges.[80]

Alkali cations in MnO_2, filled into the large tunnels (2 × 2) of α-MnO_2 and interlayer space (~7 Å) of δ-MnO_2, may also play an important role in the oxidative reactivity of MnO_2.[77,81,82] Researchers have shown that higher K contents in OMS-2 would enhance the catalytic oxidation of benzene.[83] As shown in Table 1, the K-to-Mn ratio of δ-MnO_2 is higher than that of α-MnO_2,[77,78] while the K-to-Mn ratio of γ-MnO_2 and β-MnO_2 is 0.[77] For γ-MnO_2, the synthesis method did not contain K; therefore, its K-to-Mn ratio is 0. The K-to-Mn ratios of MnO_2 decreased in the order of δ-MnO_2 > α-MnO_2 > γ-MnO_2 = β-MnO_2, which, to some extent, is in agreement with their oxidative reactivity. This is mainly because K^+ can compensate for the charges of the reduced Mn state, such that the K-to-Mn ratio can correlate with the contents of different Mn oxidation states [low K-to-Mn ratios lead to high Mn(IV) content].[10] In addition to Mn(III) defects, there are also oxygen defects[10] or Mn(IV) vacancies that may also affect K contents. Studies showed that the Mn vacancies in AMO can undergo deprotonation and, hence, facilitate proton coupled electron transfer in WO catalysis, while a perfectly filled Mn^{3+}/Mn^{4+} MnO_2 sheet showed poor catalytic activity in WO.[14,84]

It is important to recognize that some of the MnO_2 structural properties are highly related. In addition to the K-to-Mn ratio versus Mn AOS, as discussed above, Mn AOS and lattice oxygen availability may be related because when lattice oxygen is involved in catalytic reaction, the Mn−O bond strength [depending on the abundance of Mn(III)-O versus Mn(IV)-O bonds] will affect the ease of reversibility of the lattice oxygen, and the easy release of lattice oxygen would promote the oxidation ability.[85] MnO_2 surface energy was also found to generally decrease with decreasing Mn AOS, which would enhance their stability and functionality.[86] Our observed linear correlation between Mn AOS and the k values of the MnO_2 suggests that the MnO_2 surface energy might also be important in MnO_2 oxidative reactivity.

Finally, MnO_2 with longer Mn−O bonds has lower Mn−O bond strength. The average Mn−O distance of α-, β-, γ-, and δ-MnO_2 is 1.925, 1.888, 1.91, and 1.936 Å, respectively,[15,47] which, to some extent, could explain the oxidative reactivity decrease in the order of δ-MnO_2 > α-MnO_2 > γ-MnO_2> β-MnO_2. This is probably because larger fractions of Mn(III) in MnO_2 yielded longer Mn−O bonds. The exception is λ-MnO_2, which has the longest Mn−O bond length (1.962 Å).[15] Its low activity may be dominated by its low surface Mn(III) content (20.6%, Table 1).

Environmental Significance. Because the amount and types of OCs discharged into the environment continue to grow, it is imperative to develop cost-effective treatment technologies targeting OCs removal during water and wastewater treatment and at contaminated sites. The examination of the properties and reactivity of a range of synthetic MnO_2 will enable us to synthesize suitable materials to oxidize OCs efficiently. Due to the better oxidative performance and facile preparation processes, δ- and α-MnO_2 may be used as cost-effective MnO_2 in water and wastewater treatment. Potential remediation strategies can also be developed based on the findings of this work. For example, in situ degradation of OCs can be stimulated by dosing necessary species that can facilitate fast degradation kinetics. Given the importance of MnO_2 in the abiotic transformation of OCs in the environment, understanding the structure and property-dependent reactivity of various MnO_2 will also provide vital information in predicting the environmental fate of OC.

DOI: 10.1021/acs.est.8b03383
Environ. Sci. Technol. XXXX, XXX, XXX−XXX

■ ASSOCIATED CONTENT

Supporting Information

The Supporting Information is available free of charge on the ACS Publications website at DOI: 10.1021/acs.est.8b03383.

Additional details on chemicals and reagents, the synthesis of manganese oxides, and the characterization and reactivity calculation; tables showing characteristics of the examined manganese oxide, elemental values, and subset regression; Figures showing SEM and HRTEM images, manganese oxide characteristic relationships, cyclic voltammograms, spectral measurements, oxidative degradation, and SEM−EDX measurements (PDF)

■ AUTHOR INFORMATION

Corresponding Author

*Phone: 216-368-0689; e-mail: hjz13@case.edu.

ORCID

Yifan Dai: 0000-0002-1009-5790

Chung-Chiun Liu: 0000-0002-4313-8064

Huichun Zhang: 0000-0002-5683-5117

Author Contributions

§J.H. and S.Z. contributed equally to this work.

Notes

The authors declare no competing financial interest.

■ ACKNOWLEDGMENTS

This material is based on work supported by the National Science Foundation under grant nos. CBET-1762691 and CHE-1808406 to H.Z. The authors are thankful to Dr. Kevin Abbasi at the Case Western Reserve University and Dr. José M. Cerrato at University of New Mexico for assistance in XPS analysis and to Dr. Burcu Gurkan at Case Western Reserve University for allowing access to her BET instrument.

■ REFERENCES

(1) Xiong, W.; Sun, Y.; Ding, X.; Wang, M.; Zeng, Z. Selective pressure of antibiotics on ARGs and bacterial communities in manure-polluted freshwater-sediment microcosms. *Front. Microbiol.* **2015**, *6*, 194.

(2) Kabir, E. R.; Rahman, M. S.; Rahman, I. A review on endocrine disruptors and their possible impacts on human health. *Environ. Toxicol. Pharmacol.* **2015**, *40* (1), 241−258.

(3) Vidal, C. B.; Seredych, M.; Rodríguez-Castellón, E.; Nascimento, R. F.; Bandosz, T. J. Effect of nanoporous carbon surface chemistry on the removal of endocrine disruptors from water phase. *J. Colloid Interface Sci.* **2015**, *449*, 180−191.

(4) Lin, K.; Liu, W.; Gan, J. Oxidative removal of bisphenol A by manganese dioxide: efficacy, products, and pathways. *Environ. Sci. Technol.* **2009**, *43* (10), 3860−3864.

(5) Zhang, H.; Huang, C.-H. Oxidative transformation of triclosan and chlorophene by manganese oxides. *Environ. Sci. Technol.* **2003**, *37* (11), 2421−2430.

(6) Zhang, H.; Taujale, S.; Huang, J.; Lee, G.-J. Effects of NOM on oxidative reactivity of manganese dioxide in binary oxide mixtures with goethite or hematite. *Langmuir* **2015**, *31* (9), 2790−2799.

(7) Lu, X.; Zhai, T.; Zhang, X.; Shen, Y.; Yuan, L.; Hu, B.; Gong, L.; Chen, J.; Gao, Y.; Zhou, J.; Tong, Y.; Wang, Z. L.; et al. WO_3−x@Au@ MnO_2 Core−Shell Nanowires on Carbon Fabric for High-Performance Flexible Supercapacitors. *Adv. Mater.* **2012**, *24* (7), 938−944.

(8) Stone, A. T. Reductive dissolution of manganese (III/IV) oxides by substituted phenols. *Environ. Sci. Technol.* **1987**, *21* (10), 979−988.

(9) Taujale, S.; Baratta, L. R.; Huang, J.; Zhang, H. Interactions in ternary mixtures of MnO_2, Al_2O_3, and natural organic matter (NOM) and the impact on MnO_2 oxidative reactivity. *Environ. Sci. Technol.* **2016**, *50* (5), 2345−2353.

(10) Meng, Y.; Song, W.; Huang, H.; Ren, Z.; Chen, S.-Y.; Suib, S. L. Structure−property relationship of bifunctional MnO_2 nanostructures: highly efficient, ultra-stable electrochemical water oxidation and oxygen reduction reaction catalysts identified in alkaline media. *J. Am. Chem. Soc.* **2014**, *136* (32), 11452−11464.

(11) Zaharieva, I.; Chernev, P.; Risch, M.; Klingan, K.; Kohlhoff, M.; Fischer, A.; Dau, H. Electrosynthesis, functional, and structural characterization of a water-oxidizing manganese oxide. *Energy Environ. Sci.* **2012**, *5* (5), 7081−7089.

(12) Indra, A.; Menezes, P. W.; Zaharieva, I.; Baktash, E.; Pfrommer, J.; Schwarze, M.; Dau, H.; Driess, M. Active Mixed-Valent MnOx Water Oxidation Catalysts through Partial Oxidation (Corrosion) of Nanostructured MnO Particles. *Angew. Chem., Int. Ed.* **2013**, *52* (50), 13206−13210.

(13) Peng, H.; McKendry, I. G.; Ding, R.; Thenuwara, A. C.; Kang, Q.; Shumlas, S. L.; Strongin, D. R.; Zdilla, M. J.; Perdew, J. P. Redox properties of birnessite from a defect perspective. *Proc. Natl. Acad. Sci. U. S. A.* **2017**, *114* (36), 9523−9528.

(14) Birkner, N.; Nayeri, S.; Pashaei, B.; Najafpour, M. M.; Casey, W. H.; Navrotsky, A. Energetic basis of catalytic activity of layered nanophase calcium manganese oxides for water oxidation. *Proc. Natl. Acad. Sci. U. S. A.* **2013**, *110* (22), 8801−8806.

(15) Robinson, D. M.; Go, Y. B.; Mui, M.; Gardner, G.; Zhang, Z.; Mastrogiovanni, D.; Garfunkel, E.; Li, J.; Greenblatt, M.; Dismukes, G. C. Photochemical water oxidation by crystalline polymorphs of manganese oxides: structural requirements for catalysis. *J. Am. Chem. Soc.* **2013**, *135* (9), 3494−3501.

(16) Pokhrel, R.; Goetz, M. K.; Shaner, S. E.; Wu, X.; Stahl, S. S. The "best catalyst" for water oxidation depends on the oxidation method employed: a case study of manganese oxides. *J. Am. Chem. Soc.* **2015**, *137* (26), 8384−8387.

(17) Li, J.; Wang, R.; Hao, J. Role of lattice oxygen and lewis acid on ethanol oxidation over OMS-2 catalyst. *J. Phys. Chem. C* **2010**, *114* (23), 10544−10550.

(18) Luo, J.; Zhang, Q.; Garcia-Martinez, J.; Suib, S. L. Adsorptive and acidic properties, reversible lattice oxygen evolution, and catalytic mechanism of cryptomelane-type manganese oxides as oxidation catalysts. *J. Am. Chem. Soc.* **2008**, *130* (10), 3198−3207.

(19) Sithambaram, S.; Kumar, R.; Son, Y.-C.; Suib, S. L. Tandem catalysis: Direct catalytic synthesis of imines from alcohols using manganese octahedral molecular sieves. *J. Catal.* **2008**, *253* (2), 269−277.

(20) Genuino, H. C.; Dharmarathna, S.; Njagi, E. C.; Mei, M. C.; Suib, S. L. Gas-phase total oxidation of benzene, toluene, ethylbenzene, and xylenes using shape-selective manganese oxide and copper manganese oxide catalysts. *J. Phys. Chem. C* **2012**, *116* (22), 12066−12078.

(21) Zhao, B.; Ran, R.; Wu, X.; Weng, D. Phase structures, morphologies, and NO catalytic oxidation activities of single-phase MnO2 catalysts. *Appl. Catal., A* **2016**, *514*, 24−34.

(22) Shaikh, N.; Taujale, S.; Zhang, H.; Ali, A.-M. S.; Cerrato, J. M.; Artyushkova, K. Spectroscopic Investigation of Interfacial Interaction of Manganese Oxide with Triclosan, Aniline, and Phenol. *Environ. Sci. Technol.* **2016**, *50* (20), 10978−10987.

(23) Laha, S.; Luthy, R. G. Oxidation of aniline and other primary aromatic amines by manganese dioxide. *Environ. Sci. Technol.* **1990**, *24* (3), 363−373.

(24) Zhang, H.; Huang, C.-H. Oxidative transformation of fluoroquinolone antibacterial agents and structurally related amines by manganese oxide. *Environ. Sci. Technol.* **2005**, *39* (12), 4474−4483.

(25) Zhang, H.; Huang, C.-H. Reactivity and transformation of antibacterial N-oxides in the presence of manganese oxide. *Environ. Sci. Technol.* **2005**, *39* (2), 593−601.

DOI: 10.1021/acs.est.8b03383
Environ. Sci. Technol. XXXX, XXX, XXX−XXX

(26) Balgooyen, S.; Alaimo, P. J.; Remucal, C. K.; Ginder-Vogel, M. Structural Transformation of MnO_2 during the Oxidation of Bisphenol A. *Environ. Sci. Technol.* **2017**, *51* (11), 6053−6062.
(27) Ukrainczyk, L.; McBride, M. B. Oxidation of phenol in acidic aqueous suspensions of manganese oxides. *Clays Clay Miner.* **1992**, *40* (2), 157−166.
(28) Shin, J. Y.; Cheney, M. A. Abiotic transformation of atrazine in aqueous suspension of four synthetic manganese oxides. *Colloids Surf., A* **2004**, *242* (1), 85−92.
(29) Liu, C.; Zhang, L.; Feng, C.; Wu, C.; Li, F.; Li, X. Relationship between oxidative degradation of 2-mercaptobenzothiazole and physicochemical properties of manganese (hydro) oxides. *Environ. Chem.* **2009**, *6* (1), 83−92.
(30) Liu, C.; Zhang, L.; Li, F.; Wang, Y.; Gao, Y.; Li, X.; Cao, W.; Feng, C.; Dong, J.; Sun, L. Dependence of sulfadiazine oxidative degradation on physicochemical properties of manganese dioxides. *Ind. Eng. Chem. Res.* **2009**, *48* (23), 10408−10413.
(31) Dong, J.; Zhang, L.-j.; Liu, H.; Liu, C.-s.; Gao, Y.-x.; Sun, L.-n. The Oxidative Degradation of 2-Mercapto-benzothialzole by Different Manganese Dioxides. *Fresenius Environ. Bull.* **2010**, *19* (8), 1615−1622.
(32) Weaver, R. M.; Hochella, M. F. The reactivity of seven Mn-oxides with Cr3+ aq: A comparative analysis of a complex, environmentally important redox reaction. *Am. Mineral.* **2003**, *88* (11−12), 2016−2027.
(33) Yu, X.; Xue, J.; Yao, H.; Wu, Q.; Venkatesan, A. K.; Halden, R. U.; Kannan, K. Occurrence and estrogenic potency of eight bisphenol analogs in sewage sludge from the U.S. EPA targeted national sewage sludge survey. *J. Hazard. Mater.* **2015**, *299*, 733−739.
(34) Cerrato, J. M.; Hochella, M. F., Jr; Knocke, W. R.; Dietrich, A. M.; Cromer, T. F. Use of XPS to identify the oxidation state of Mn in solid surfaces of filtration media oxide samples from drinking water treatment plants. *Environ. Sci. Technol.* **2010**, *44* (15), 5881−5886.
(35) Lan, S.; Wang, X.; Xiang, Q.; Yin, H.; Tan, W.; Qiu, G.; Liu, F.; Zhang, J.; Feng, X. Mechanisms of Mn(II) catalytic oxidation on ferrihydrite surfaces and the formation of manganese (oxyhydr)-oxides. *Geochim. Cosmochim. Acta* **2017**, *211*, 79−96.
(36) Post, J. E.; Veblen, D. R. Crystal structure determinations of synthetic sodium, magnesium, and potassium birnessite using TEM and the Rietveld method. *Am. Mineral.* **1990**, *75* (5−6), 477−489.
(37) Zhang, J.; Li, Y.; Wang, L.; Zhang, C.; He, H. Catalytic oxidation of formaldehyde over manganese oxides with different crystal structures. *Catal. Sci. Technol.* **2015**, *5* (4), 2305−2313.
(38) Turner, S.; Buseck, P. R. Manganese oxide tunnel structures and their intergrowths. *Science* **1979**, *203* (4379), 456−458.
(39) Wan, J.; Zhou, L.; Deng, H.; Zhan, F.; Zhang, R. Oxidative degradation of sulfamethoxazole by different MnO_2 nanocrystals in aqueous solution. *J. Mol. Catal. A: Chem.* **2015**, *407*, 67−74.
(40) Yanina, S. V.; Rosso, K. M. Linked reactivity at mineral-water interfaces through bulk crystal conduction. *Science* **2008**, *320* (5873), 218−222.
(41) Handler, R. M.; Beard, B. L.; Johnson, C. M.; Scherer, M. M. Atom exchange between aqueous Fe (II) and goethite: An Fe isotope tracer study. *Environ. Sci. Technol.* **2009**, *43* (4), 1102−1107.
(42) Rosso, K. M.; Yanina, S. V.; Gorski, C. A.; Larese-Casanova, P.; Scherer, M. M. Connecting observations of hematite (α-Fe_2O_3) growth catalyzed by Fe (II). *Environ. Sci. Technol.* **2010**, *44* (1), 61−67.
(43) Santos, V.; Pereira, M.; Órfão, J.; Figueiredo, J. The role of lattice oxygen on the activity of manganese oxides towards the oxidation of volatile organic compounds. *Appl. Catal., B* **2010**, *99* (1), 353−363.
(44) Sun, M.; Lan, B.; Yu, L.; Ye, F.; Song, W.; He, J.; Diao, G.; Zheng, Y. Manganese oxides with different crystalline structures: facile hydrothermal synthesis and catalytic activities. *Mater. Lett.* **2012**, *86*, 18−20.
(45) Xie, Y.; Yu, Y.; Gong, X.; Guo, Y.; Guo, Y.; Wang, Y.; Lu, G. Effect of the crystal plane figure on the catalytic performance of MnO_2 for the total oxidation of propane. *CrystEngComm* **2015**, *17* (15), 3005−3014.
(46) Dong, Y.; Li, K.; Jiang, P.; Wang, G.; Miao, H.; Zhang, J.; Zhang, C. Simple hydrothermal preparation of α-, β-, and γ-MnO_2 and phase sensitivity in catalytic ozonation. *RSC Adv.* **2014**, *4* (74), 39167−39173.
(47) Liang, S.; Teng, F.; Bulgan, G.; Zong, R.; Zhu, Y. Effect of phase structure of MnO_2 nanorod catalyst on the activity for CO oxidation. *J. Phys. Chem. C* **2008**, *112* (14), 5307−5315.
(48) Wang, F.; Dai, H.; Deng, J.; Bai, G.; Ji, K.; Liu, Y. Manganese oxides with rod-, wire-, tube-, and flower-like morphologies: highly effective catalysts for the removal of toluene. *Environ. Sci. Technol.* **2012**, *46* (7), 4034−4041.
(49) McKendry, I. G.; Kondaveeti, S. K.; Shumlas, S. L.; Strongin, D. R.; Zdilla, M. J. Decoration of the layered manganese oxide birnessite with Mn (II/III) gives a new water oxidation catalyst with fifty-fold turnover number enhancement. *Dalton Trans.* **2015**, *44* (29), 12981−12984.
(50) Sun, M.; Lan, B.; Lin, T.; Cheng, G.; Ye, F.; Yu, L.; Cheng, X.; Zheng, X. Controlled synthesis of nanostructured manganese oxide: crystalline evolution and catalytic activities. *CrystEngComm* **2013**, *15* (35), 7010−7018.
(51) Ilton, E. S.; Post, J. E.; Heaney, P. J.; Ling, F. T.; Kerisit, S. N. XPS determination of Mn oxidation states in Mn (hydr)oxides. *Appl. Surf. Sci.* **2016**, *366* (C), 475−485.
(52) Nawaz, F.; Cao, H.; Xie, Y.; Xiao, J.; Chen, Y.; Ghazi, Z. A. Selection of active phase of MnO_2 for catalytic ozonation of 4-nitrophenol. *Chemosphere* **2017**, *168*, 1457−1466.
(53) Kang, L.; Liu, Z.-H.; Yang, Z.; Ooi, K. Simultaneous synthesis of high crystalline manganese oxides with layered and tunnel structures. *Mater. Lett.* **2006**, *60* (29−30), 3565−3568.
(54) Nico, P. S.; Zasoski, R. J. Importance of Mn (III) availability on the rate of Cr (III) oxidation on δ-MnO_2. *Environ. Sci. Technol.* **2000**, *34* (16), 3363−3367.
(55) Nico, P. S.; Zasoski, R. J. Mn (III) center availability as a rate controlling factor in the oxidation of phenol and sulfide on δ-MnO_2. *Environ. Sci. Technol.* **2001**, *35* (16), 3338−3343.
(56) Gorlin, Y.; Lassalle-Kaiser, B.; Benck, J. D.; Gul, S.; Webb, S. M.; Yachandra, V. K.; Yano, J.; Jaramillo, T. F. In situ X-ray absorption spectroscopy investigation of a bifunctional manganese oxide catalyst with high activity for electrochemical water oxidation and oxygen reduction. *J. Am. Chem. Soc.* **2013**, *135* (23), 8525−8534.
(57) Kutner, M. H.; Nachtsheim, C.; Neter, J. *Applied linear regression models*; McGraw-Hill/Irwin: New York, 2004.
(58) Maitra, U.; Naidu, B.; Govindaraj, A.; Rao, C. Importance of trivalency and the eg1 configuration in the photocatalytic oxidation of water by Mn and Co oxides. *Proc. Natl. Acad. Sci. U. S. A.* **2013**, *110* (29), 11704−11707.
(59) Takashima, T.; Hashimoto, K.; Nakamura, R. Inhibition of charge disproportionation of MnO_2 electrocatalysts for efficient water oxidation under neutral conditions. *J. Am. Chem. Soc.* **2012**, *134* (44), 18153−18156.
(60) Kuo, C. H.; Li, W.; Pahalagedara, L.; El-Sawy, A. M.; Kriz, D.; Genz, N.; Guild, C.; Ressler, T.; Suib, S. L.; He, J. Understanding the role of gold nanoparticles in enhancing the catalytic activity of manganese oxides in water oxidation reactions. *Angew. Chem., Int. Ed.* **2015**, *54* (8), 2345−2350.
(61) Mosa, I. M.; Biswas, S.; El-Sawy, A. M.; Botu, V.; Guild, C.; Song, W.; Ramprasad, R.; Rusling, J. F.; Suib, S. L. Tunable mesoporous manganese oxide for high performance oxygen reduction and evolution reactions. *J. Mater. Chem. A* **2016**, *4* (2), 620−631.
(62) Hu, E.; Zhang, Y.; Wu, S.; Wu, J.; Liang, L.; He, F. Role of dissolved Mn(III) in transformation of organic contaminants: Non-oxidative versus oxidative mechanisms. *Water Res.* **2017**, *111* (C), 234−243.
(63) Madison, A. S.; Tebo, B. M.; Mucci, A.; Sundby, B.; Luther, G. W. Abundant porewater Mn (III) is a major component of the sedimentary redox system. *Science* **2013**, *341* (6148), 875−878.

DOI: 10.1021/acs.est.8b03383
Environ. Sci. Technol. XXXX, XXX, XXX−XXX

(64) Trouwborst, R. E.; Clement, B. G.; Tebo, B. M.; Glazer, B. T.; Luther, G. W. Soluble Mn (III) in suboxic zones. *Science* **2006**, *313* (5795), 1955−1957.
(65) Kostka, J. E.; Luther, G. W., III; Nealson, K. H. Chemical and biological reduction of Mn (III)-pyrophosphate complexes: potential importance of dissolved Mn (III) as an environmental oxidant. *Geochim. Cosmochim. Acta* **1995**, *59* (5), 885−894.
(66) Wang, Y.; Stone, A. T. The citric acid−Mn(III, IV)O_2 (birnessite) reaction. Electron transfer, complex formation, and autocatalytic feedback. *Geochim. Cosmochim. Acta* **2006**, *70* (17), 4463−4476.
(67) McArdell, C. S.; Stone, A. T.; Tian, J. Reaction of EDTA and related aminocarboxylate chelating agents with CoIIIOOH (heterogenite) and MnIIIOOH (Manganite). *Environ. Sci. Technol.* **1998**, *32* (19), 2923−2930.
(68) Klewicki, J.; Morgan, J. Dissolution of β-MnOOH particles by ligands: pyrophosphate, ethylenediaminetetraacetate, and citrate. *Geochim. Cosmochim. Acta* **1999**, *63* (19), 3017−3024.
(69) Wang, Z.; Xiong, W.; Tebo, B. M.; Giammar, D. E. Oxidative UO_2 Dissolution Induced by Soluble Mn(III). *Environ. Sci. Technol.* **2014**, *48* (1), 289−298.
(70) Chen, W.-R.; Liu, C.; Boyd, S. A.; Teppen, B. J.; Li, H. Reduction of carbadox mediated by reaction of Mn (III) with oxalic acid. *Environ. Sci. Technol.* **2013**, *47* (3), 1357−1364.
(71) Kolling, D. R.; Cox, N.; Ananyev, G. M.; Pace, R. J.; Dismukes, G. C. What are the oxidation states of manganese required to catalyze photosynthetic water oxidation? *Biophys. J.* **2012**, *103* (2), 313−322.
(72) Gao, Y.; Jiang, J.; Zhou, Y.; Pang, S.-Y.; Jiang, C.; Guo, Q.; Duan, J.-B. Does Soluble Mn(III) Oxidant Formed in Situ Account for Enhanced Transformation of Triclosan by Mn(VII) in the Presence of Ligands? *Environ. Sci. Technol.* **2018**, *52* (8), 4785−4793.
(73) Manceau, A.; Silvester, E.; Bartoli, C.; Lanson, B.; Drits, V. A. Structural mechanism of Co2+ oxidation by the phyllomanganate buserite. *Am. Mineral.* **1997**, *82* (11−12), 1150−1175.
(74) Yu, Q.; Sasaki, K.; Tanaka, K.; Ohnuki, T.; Hirajima, T. Structural factors of biogenic birnessite produced by fungus Paraconiothyrium sp. WL-2 strain affecting sorption of Co^{2+}. *Chem. Geol.* **2012**, *310*, 106−113.
(75) Simanova, A. A.; Peña, J. Time-Resolved Investigation of Cobalt Oxidation by Mn(III)-Rich δ-MnO_2 Using Quick X-ray Absorption Spectroscopy. *Environ. Sci. Technol.* **2015**, *49* (18), 10867−10876.
(76) Bergmann, A.; Zaharieva, I.; Dau, H.; Strasser, P. Electrochemical water splitting by layered and 3D cross-linked manganese oxides: correlating structural motifs and catalytic activity. *Energy Environ. Sci.* **2013**, *6* (9), 2745−2755.
(77) Boppana, V. B. R.; Yusuf, S.; Hutchings, G. S.; Jiao, F. Nanostructured Alkaline-Cation-Containing δ-MnO_2 for Photocatalytic Water Oxidation. *Adv. Funct. Mater.* **2013**, *23* (7), 878−884.
(78) Duan, X.; Yang, J.; Gao, H.; Ma, J.; Jiao, L.; Zheng, W. Controllable hydrothermal synthesis of manganese dioxide nanostructures: shape evolution, growth mechanism and electrochemical properties. *CrystEngComm* **2012**, *14* (12), 4196−4204.
(79) Yuan, J.; Laubernds, K.; Zhang, Q.; Suib, S. L. Self-assembly of microporous manganese oxide octahedral molecular sieve hexagonal flakes into mesoporous hollow nanospheres. *J. Am. Chem. Soc.* **2003**, *125* (17), 4966−4967.
(80) Saputra, E.; Muhammad, S.; Sun, H.; Ang, H. M.; Tade, M.; Wang, S. Different crystallographic one-dimensional MnO_2 nanomaterials and their superior performance in catalytic phenol degradation. *Environ. Sci. Technol.* **2013**, *47* (11), 5882−5887.
(81) Tao, L.; Stich, T. A.; Jaccard, H.; Britt, R. D.; Casey, W. H. Manganese-Oxide Solids as Water-Oxidation Electrocatalysts: The Effect of Intercalating Cations. In *Advances in the Environmental Biogeochemistry of Manganese Oxides*; American Chemical Society: Washington, DC, 2015; Vol. *1197*, pp 135−153.
(82) Biswas, S.; Poyraz, A. S.; Meng, Y.; Kuo, C.-H.; Guild, C.; Tripp, H.; Suib, S. L. Ion induced promotion of activity enhancement of mesoporous manganese oxides for aerobic oxidation reactions. *Appl. Catal., B* **2015**, *165*, 731−741.
(83) Hou, J.; Liu, L.; Li, Y.; Mao, M.; Lv, H.; Zhao, X. Tuning the K^+ concentration in the tunnel of OMS-2 nanorods leads to a significant enhancement of the catalytic activity for benzene oxidation. *Environ. Sci. Technol.* **2013**, *47* (23), 13730−13736.
(84) Iyer, A.; Del-Pilar, J.; King'ondu, C. K.; Kissel, E.; Garces, H. F.; Huang, H.; El-Sawy, A. M.; Dutta, P. K.; Suib, S. L. Water oxidation catalysis using amorphous manganese oxides, octahedral molecular sieves (OMS-2), and octahedral layered (OL-1) manganese oxide structures. *J. Phys. Chem. C* **2012**, *116* (10), 6474−6483.
(85) Makwana, V. D.; Son, Y.-C.; Howell, A. R.; Suib, S. L. The role of lattice oxygen in selective benzyl alcohol oxidation using OMS-2 catalyst: a kinetic and isotope-labeling study. *J. Catal.* **2002**, *210* (1), 46−52.
(86) Birkner, N.; Navrotsky, A. Thermodynamics of manganese oxides: Sodium, potassium, and calcium birnessite and cryptomelane. *Proc. Natl. Acad. Sci. U. S. A.* **2017**, *114* (7), E1046−E1053.

DOI: 10.1021/acs.est.8b03383
Environ. Sci. Technol. XXXX, XXX, XXX−XXX